



Science Arts & Métiers (SAM)

is an open access repository that collects the work of Arts et Métiers Institute of Technology researchers and makes it freely available over the web where possible.

This is an author-deposited version published in: <https://sam.ensam.eu>
Handle ID: <http://hdl.handle.net/10985/17207>

To cite this version :

Jean-Christophe OLIVIER, Christophe JOSSET, AUVITY, Stéphane CHEVALIER - Polymer electrolyte membrane fuel cell operating in stoichiometric regime - Journal of Power Sources - Vol. 440, p.227100 - 2019

Any correspondence concerning this service should be sent to the repository

Administrator : scienceouverte@ensam.eu



Polymer electrolyte membrane fuel cell operating in stoichiometric regime

S. Chevalier^{a,*}, J.-C. Olivier^b, C. Josset^c, B. Auvity^c

^a I2M - Institut de Mécanique et d'Ingénierie de Bordeaux (CNRS UMR 5295) École Nationale Supérieure d'Arts et Métiers (ENSAM), Esplanade des Arts et Métiers, 33405, Talence Cédex, France

^b IREENA Laboratory (EA 4642), Université de Nantes, 37 boulevard de l'université, BP 406, 44602, Saint-Nazaire Cedex, Saint-Nazaire, France

^c Laboratoire de Thermique et Énergie de Nantes (CNRS UMR 6607), Polytech Nantes, Université de Nantes, La Chantrerie, rue Christian Pauc - CS 50609, 44306, Nantes Cedex 3, France

HIGHLIGHTS

- Fuel cell stoichiometric regime is evidenced at global and local scale.
- Cathode channel mass transport governs the fuel cell performance in this regime.
- Low frequency spectral signature of stoichiometric regime is measured using EIS.
- Current density distributions are measured using a segmented flow field.
- Fuel cell kinetic parameters can be easily measured in stoichiometric regime.

ARTICLE INFO

Keywords:

Stoichiometric regime
Analytical model
Segmented cell
PEM fuel cell
EIS

ABSTRACT

In this work, we report the existence of a stoichiometric regime where the performances of operating polymer electrolyte membrane (PEM) fuel cells are entirely governed by the mass transport in the cathode channels. An analytical model of the fuel cell stoichiometric regime is derived and evidenced experimentally: from the cell spectral signature at low frequency based on electrochemical impedance spectroscopy, and from the current density distribution measured using a segmented current collector. The existence of such regime provides a simple way to characterize, model and predict PEM fuel cell performances.

1. Introduction

Alternative engines to convert and store energy which do not produce any greenhouse gas are a must need. Among the large variety of processes such as wind turbine or solar panel for example, Polymer Electrolyte Membrane (PEM) fuel cells are one of the most promising candidates. They convert hydrogen and air into electricity and heat with water as the only by-product. The efficiency of the direct conversion of the chemical energy into electrical energy is also an important asset of this technology. Today, PEM fuel cells are close to the commercialization, but their cost still needs to be decreased to reach the full market deployment [1,2]. To make the fuel cells less costly, one way is to increase the electrical power density for a given cell. This can be achieved by both improving the electrochemistry [3] and the mass transport in all the fuel cell materials [4].

To study and improve the mass transport in fuel cells, numerous numerical models have been developed by the research community from

the cell scale to the pore scale in the GDL or in the catalyst layer [5–7]. Comprehensive reviews of fuel cell mass transport mechanisms are available in the literature [4,8,9] which summarise all the recent advances in fuel cell modeling. An ubiquitous drawback to all the models reported in the previous references is the large number of parameters required (more than ten in general, see Refs. [10,11] for example). If few of them can be easily obtained such as the cell dimensions, or operating conditions, most parameters related to the GDL properties (conductivity, permeability), catalyst layer properties (kinetic reaction coefficients) or PEM properties (drag coefficient [12], ionic conductivity) are – in most cases – not accurately known, which introduce a lot of uncertainty in fuel cell model results. In this context, and to overcome this problem, some authors have developed simplified models which rely onto a very limited sets of fuel cell parameters [13–20]. Such less parametrised models usually work under strong assumptions and over a limited range of operating regimes – which allow for neglecting some of the fuel cell phenomena such as the anode electrochemical reactions for example. In counter part, these simplified models are well suited to make accurate

* Corresponding author.

E-mail address: stephane.chevalier@u-bordeaux.fr (S. Chevalier).

Nomenclature

Parameters and variables

b	V, Tafel slope
c_c	mol/m ³ , oxygen concentration in the channel
c^{ref}	mol/m ³ , Reference concentration at the channel inlet
Da	Damkholer number
D^{eff}	m ² /s, Effective diffusivity of the GDL
E_{cell}	V, Fuel cell potential
F	C/mol, Faraday constant
h_c	m, Channel depth
h_g	m, GDL thickness
i	Complex unity
i_c	mA/cm ² , Exchange current density
I_{cell}	A/cm ² , Fuel cell current density measured by the FC station
j	A/cm ² , Local current density
j_0	A/cm ² , Inlet current density
l_c	m, Cell width
L_c	m, Channel length
M	g/mol, Molar mass
Pe	Peclet number
\dot{Q}	ml/min, Air flow rate in operating pressure and

	temperature
\dot{Q}_{SCEPT}	ml/min, Air flow rate in standard condition of pressure and temperature
r_{HF}	m Ω , Fuel cell ohmic resistance
R	J/mol/K, Ideal gas constant
R_{ct}	$\Omega \cdot \text{cm}^2$, Charge transfer resistance
T	K, Temperature
u_c	m/s, Air velocity
Wa	Wagner number
x	Molar fraction
y	m, Spatial coordinate
Z	$\Omega \cdot \text{cm}^2$, Complex fuel cell impedance

Greek letter

α_c	Dimensionless charge transfer coefficient
δ	Periodic state
φ	$^\circ$, Phase
η	V, Overpotential in the CL
λ	Oxygen stoichiometry
ρ	kg/m ³ , Density
τ	s, Characteristic time
ω	rad/s, Angular frequency

fuel cell properties measurements such as electrochemical properties.

Alongside fuel cell model developments, experimental characterizations of fuel cell properties have been widely reported in the literature. These works were focused at different scales: from the system scale where a whole fuel cell stack is studied [21,22], to component scale where the liquid water transport was imaged in the GDL pores via X-rays radiography for example [23–26]. In between, the single fuel cell behaviour was also studied using mainly electrochemical techniques such as Electrochemical Impedance Spectroscopy (EIS) [27]. This technique is particularly well suited to characterize fuel cell kinetics [28], membrane resistance [29] and mass transport in both GDLs and channels [16,30,31]. A comprehensive review of the fuel cell phenomena which can be characterized through EIS is given in Ref. [32]. However, EIS applied to the cell gives a global characterization of the physical phenomena whereas it is well admitted that the fuel cell properties can change along the channel [33,34]. Thus, segmented fuel cells were developed in order to measure local current densities [35] and to perform local electrochemical characterizations [33]. Different designs of segmented fuel cell were developed, using segmented straight channels [36], serpentine channels [37], or combining segmented fuel cell with optical visualisations [38]. In all the previous works, the great interest of segmented fuel cells was clearly proven to study the local changes of fuel cell current density, water concentration, or temperature.

In authors' previous works [16], it was shown that a stoichiometric regime can be identified in operating fuel cells. Such regime appears at low to moderate current density (less than 1 A/cm²) when the mass transport limitations in the GDL can be neglected [15,16,39]. It can be identified using the EIS signature at low frequency (between 3 and 0.5 Hz). It was shown that this low frequency signature is a consequence of the oxygen transport in the channel [40] which is different from the inductive low frequency behavior pointed out by Pivac et al. [41,42] to monitor fuel cell aging. Low frequency capacitive loop can also be observed in case of dehydrated membrane as reported by Chevalier et al. [43], but at frequency lower than 1 Hz and in case of very dry operating conditions. Therefore, low frequency capacitive loop measured at low stoichiometry using relatively well hydrated membrane are likely related to oxygen transport in the channel.

Going further, we extend these previous works [16,39] to the local

scale, where the current density distribution should depend only on the oxygen stoichiometry in the stoichiometric regime [44]. A segmented fuel cell was specially designed to measure the current density distributions. Once the stoichiometric regime clearly identified, a methodology to characterize the fuel cell electrochemical properties (Tafel slope and exchange current density) is derived from the equations of this fuel cell operating regime. These findings answer the need of less parametrised models for accurate fuel cell properties characterisations and bring two original results compared to the authors' previous works: (i) the evidence of a stoichiometric regime at the local scale (through current density distribution), and (ii) a methodology to accurately characterize the fuel cell kinetics parameters under the stoichiometric regime.

Subsequently in the paper, what is called the global scale is the cell scale at which the cell impedance is measured. The local scale designates the channel scale at which the segmented current density measurements are performed.

2. Methods

2.1. Current density distribution in the stoichiometric regime

The analytical model used to describe the current density and the low frequency impedance in stoichiometric regime is derived from the authors' previous work [15,16]. It was shown that under the assumption of negligible performance losses at the anode and the absence of liquid water in GDLs and channels, fuel cell models can be reduced to a simplified model governed by three dimensionless parameters. The Wagner number, $Wa = b/(r_{\Omega}j_0)$, which compares the voltage losses in the CL to the voltage losses in the membrane. The Damkholer number, $Da = i_c e^{(E^0 - E)/b} h_g / (4Fc^{ref} D^{eff})$, which compares the kinetics of the reaction to diffusive flux of oxygen in the GDL. And the Peclet number, $Pe = u_c h_c h_g / (D^{eff} L_c)$, which compares the ratio of oxygen transported in the channel to the mass transport in fuel cell porous media. At low current density and low membrane resistance, the stoichiometric regime exists for a particular set of these parameter values, i.e. when the Wagner number is found to be large enough to neglect the overpotential gradients along the channel in the PEM, and when the Damkholer is small enough to neglect the concentration gradient in the GDL, i.e. the oxygen

concentration in the CL is equal to the one in the channel. Under these conditions, the fuel cell is assumed to be operating in the stoichiometric regime [6,15,39], and the fuel cell geometry can be simplified as depicted in Fig. 1. Thus, in the stoichiometric regime, the fuel cell can be viewed as a flow field directly in contact with the catalyst layer; the GDL has no impact onto the fuel cell performances since the concentration gradients in the GDL are neglected as well as its ohmic losses.

The other main assumptions of the model concern the transport of liquid water and the value of the fuel cell parameters. In the present model, the liquid water is not explicitly modelled. It is considered that its impact can be seen through the values of the fuel cell parameters, such as the PEM ohmic resistance or the catalyst layer kinetics among others. In addition, fuel cell parameters are considered to be effective values which are constant along the channel (y-direction in Fig. 1(b)). To simplify the calculations and the model, we also consider that the fuel cell is isothermal with ideal current collectors (no ohmic losses in them). The oxygen transport in the channel is assumed to be a plug-flow with an averaged air velocity, u_c . In addition, a plane CL is considered at the cathode, meaning that the electrochemical reaction takes place homogeneously throughout the CL thickness. This last assumption is valid in case of rapid oxygen and charge transport in the CL [14]. Finally, the present stoichiometric model takes into account only the slowest transient phenomena occurring in fuel cells, i.e. the charging/discharging phenomenon in the double capacity layer is neglected.

Thus, under all these assumptions, a relatively simple expression of the transient current density distribution can be written as:

$$j(y, t) = i_c \frac{c_c(y, t)}{c_{ref}} e^{\eta(t)/b}, \quad (1)$$

where j is the current density, i_c is the exchange current density, c_c is the oxygen concentration in the channel, η is the overpotential, and b is the Tafel slope. The transport of the oxygen concentration in the channel is governed as follows:

$$\frac{\partial c_c}{\partial t}(y, t) + u_c \frac{\partial c_c}{\partial y}(y, t) = -\frac{j(y, t)}{4Fh_c}, \quad (2)$$

where u_c is the air velocity, F is the Faraday constant and h_c stands for the channel depth. Equations (1) and (2) are rewritten in dimensionless form using the following parameters: $\tilde{j} = j/j_0$ where $j_0 = j(0)$ is the inlet current density, $\tilde{c}_c = c_c/c^{ref}$, $\tilde{\eta} = \eta/b$, $\tilde{y} = y/L_c$, and $\tilde{t} = t/\tau_c$ where $\tau_c = L_c/u_c$ is the oxygen residence time in the fuel cell. Notice that in this model, the oxygen velocity, u_c , is the 2D velocity of the oxygen that would flow in a cell without ribs [16] since these latter are not taking

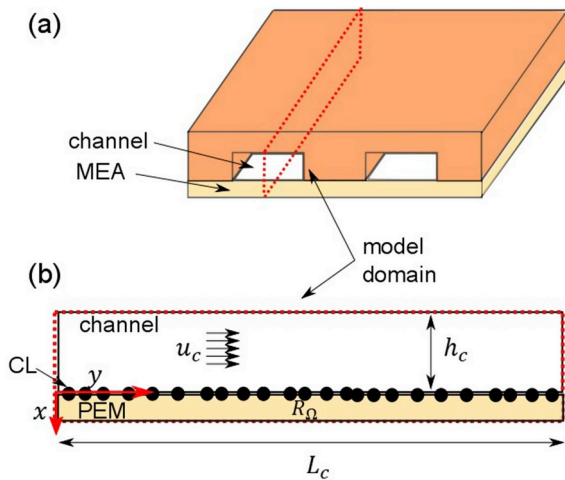


Fig. 1. Simplified geometry of a fuel cell operating in stoichiometric regime (GDL neglected). (a), 3D view of a fuel cell with two parallel channels. (b), 2D geometry used to model the fuel cell mass transport phenomena.

parameters, it leads to:

$$\tilde{j} = \alpha_c \tilde{c}_c, \quad (3)$$

where $\alpha_c = i_c/j_0 e^{\eta(t)/b}$, and

$$\frac{\partial \tilde{c}_c}{\partial \tilde{t}} + \frac{\partial \tilde{c}_c}{\partial \tilde{y}} = -\lambda^* \tilde{j}, \quad (4)$$

where $\lambda^* = j_0 L_c / (4F c^{ref} u_c h_c)$. A more convenient expression of λ^* is given at the end of this subsection, see Equation (8).

In periodic regime, equations (3) and (4) can be decomposed into steady part (real, denoted with the superscript 0) and a periodic part (complex, denoted with δ) in the frequency domain as:

- $\tilde{j}(\tilde{y}, \tilde{t}) = \tilde{j}^0(\tilde{y}) + \delta \tilde{j}(\tilde{y}, \tilde{\omega}) e^{i\tilde{\omega}\tilde{t}}$, where $\tilde{\omega} = \omega\tau_c$, $\tilde{\omega}$ is the dimensionless frequency, and ω is the angular frequency;
- $\tilde{c}_c(\tilde{y}, \tilde{t}) = \tilde{c}_c^0(\tilde{y}) + \delta \tilde{c}_c(\tilde{y}, \tilde{\omega}) e^{i\tilde{\omega}\tilde{t}}$;
- $\tilde{\eta}(\tilde{t}) = \tilde{\eta}^0 + \delta \tilde{\eta}(\tilde{\omega}) e^{i\tilde{\omega}\tilde{t}}$;
- $\alpha_c(\tilde{t}) = \alpha_c^0 (1 + \delta \tilde{\eta}(\tilde{\omega}) e^{i\tilde{\omega}\tilde{t}})$, where $\alpha_c^0 = i_c/j_0 e^{\eta^0/b}$.

Before to be solved in periodic regime, equations (3) and (4) are solved in steady states. Using the inlet conditions $\tilde{c}_c^0(0) = 1$ and $\tilde{j}^0(0) = 1$, it implies that $\alpha_c^0 = 1$ and $\tilde{c}_c^0 = \tilde{j}^0$. So, the steady state equation of the current density distribution writes

$$\tilde{j}^0(\tilde{y}) = e^{-\lambda^* \tilde{y}}. \quad (5)$$

Then, a relationship between λ^* and the oxygen stoichiometric, λ , can be found by computing the mean current density produced by the cell as

$$I_{cell} = j_0 \int_0^1 \tilde{j}^0(\tilde{y}) d\tilde{y} = \frac{j_0}{\lambda^*} (1 - e^{-\lambda^*}) \quad (6)$$

Rearranging Equation (6) with the definition of λ^* given in equation (4) leads to

$$\frac{I_{cell} \lambda^*}{j_0} = \frac{I_{cell} L_c}{4F c^{ref} u_c h_c} = \lambda^{-1}, \quad (7)$$

and by combining equations (6) and (7) one can write

$$\lambda^* = -\ln(1 - \lambda^{-1}). \quad (8)$$

Finally, a convenient expression of the current density distribution, $\tilde{j}^0(\tilde{y})$, which depends only on the oxygen stoichiometry is found by combining Equations (2), (4) and (6) as

$$\frac{\tilde{j}^0(\tilde{y})}{I_{cell}} = \lambda^* \lambda e^{-\lambda^* \tilde{y}}. \quad (9)$$

A similar expression for the current density distribution was reported by Kulikovskiy [6].

2.2. Low frequency spectral signature in stoichiometric regime

Equations (3) and (4) are now solved in the periodic regime. Using the complex decomposition previously introduced, the periodic state of Equation (1) writes

$$\delta \tilde{j} = \delta \tilde{c}_c + e^{-\lambda^* \tilde{y}} \delta \tilde{\eta}. \quad (10)$$

where $\delta \tilde{c}_c$ is obtained from the periodic state of equation (2) as:

$$i\tilde{\omega} \delta \tilde{c}_c + \frac{d}{d\tilde{y}} \delta \tilde{c}_c = -\lambda^* \delta \tilde{j}, \quad (11)$$

Combining (10) and (11), and solving them, using the inlet condition $\tilde{\delta j}(0) = 0$, leads to the following expression of the periodic current density:

$$\tilde{\delta j}(\tilde{y}) = i\lambda^* \tilde{\delta \eta} \frac{\tilde{\omega}}{\tilde{\omega}} \left(\left(1 - \frac{i\tilde{\omega}}{\lambda^*} \right) e^{-\lambda^* \tilde{y}} - e^{-\lambda^* \tilde{y} (1 + i\tilde{\omega}/\lambda^*)} \right) \quad (12)$$

Finally, one can compute the dimensionless fuel cell impedance \tilde{Z} , whose expression can be obtained from the following equation:

$$\frac{1}{\tilde{Z}} = \int_0^1 \frac{\tilde{\delta j}(\tilde{y})}{\tilde{\delta \eta}} d\tilde{y}, \quad (13)$$

developing equation (13) leads to:

$$\frac{1}{\tilde{Z}} = \frac{i}{\tilde{\omega}} \left[\left(1 - \frac{i\tilde{\omega}}{\lambda^*} \right) (1 - e^{-\lambda^*}) - \frac{1 - e^{-\lambda^* (1 + i\tilde{\omega}/\lambda^*)}}{1 + i\tilde{\omega}/\lambda^*} \right]. \quad (14)$$

Equation (14) describes the low frequency impedance of the fuel cell in the stoichiometric regime. This equation is identical to the impedance

reported in Ref. [16] when $Da \ll 1$ which is the case in such stoichiometric regime. Moreover, like the current density in steady state, it is interesting to note that this dimensionless impedance is governed only by the oxygen stoichiometry.

From equation (14), two quantities can be computed, namely the phase and the modulus of the impedance. The phase of the impedance Z is then defined as:

$$\tan \varphi = \frac{\text{Im}(1/\tilde{Z})}{\text{Re}(1/\tilde{Z})}, \quad (15)$$

and one can notice that this quantity is function of τ_c and λ only. Therefore, only the knowledge of the fuel cell operating conditions (air flow rate, pressure, temperature and current) is required to predict the fuel cell phase in stoichiometric regime. This latter will be used in the results section to evidence the stoichiometric regime. In contrast, the modulus is computed as:

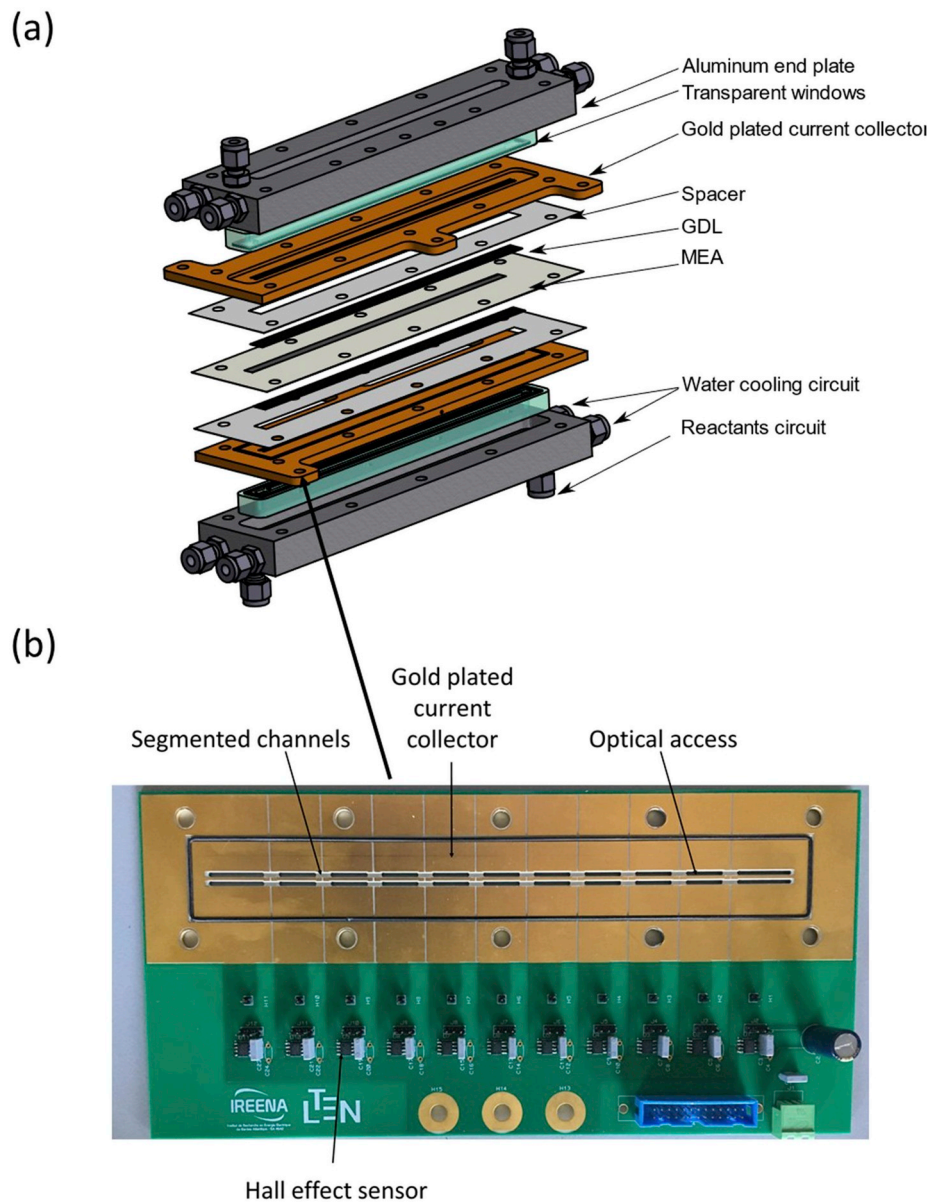


Figure 2. (a) 3D rendering view of the single cell used in the experiments. (b), segmented current collector used to measure the current density distribution. It replaces one of the copper current collector in the single cell.

$$|Z| = \left| \frac{R_{ct}}{\bar{Z}(\tau_c, \lambda)} \right|^{-1}, \quad (16)$$

with $R_{ct} = b/j_0$. Thus, the modulus is governed by τ_c , λ , and the cell electrochemical parameters. In absence of knowledge of b and j_0 it is not possible to predict the modulus of the stoichiometric regime. However, Equation (16) is used at the end the next section to validate the model after measuring the Tafel slope.

2.3. Experimental measurements

Two kinds of experiments are performed in this study to validate both the steady state model using the current density distribution measurements and the periodic state using the EIS response of the fuel cell. To measure the local current density distributions, a segmented flow field was built directly onto a printed circuit board (PCB), see Fig. 2, where the current is measured through eleven segments. Each segment is connected in series to a Hall effect current sensor (Allegro Microsystem, ACS723LLCTR-05AB-T), which converts the current that flows through the segment into voltage. All the 11 voltages are then read by a data acquisition system every second. Each sensor was carefully calibrated prior to the fuel cell current measurements (see section S1 in supplementary material). According to the datasheet of the sensor and all the experimental uncertainties, it is assumed that the current densities are measured with an accuracy of $\pm 10\%$. Such uncertainty was also verified when comparing the current measured by the segmented flow field to the current read by the fuel cell test station (see details in the supplementary materials).

The position, the area and the length of each segment are summarized in Table 1. The segmented flow field was gold plated to ensure minimal contact resistance and to prevent copper oxidation when placed inside the cell. Holes were drilled into the flow field to allow an optical access and verify that no liquid water was present in the channel as assumed in the model. The segmented flow field is inserted at the anode side.

The second kind of measurements are the classical EIS. To do so, the fuel cell was connected to a FCT 50 test station (BioLogic®) to measure the cell current, voltage and impedance. The fuel cell impedance was recorded from 10 kHz to 0.1 Hz with 10 points per decade using an AC sine wave signal equal to 10% of the DC current. The FCT 50 test station was also used to control air and hydrogen flow rates, temperatures, humidity and pressure. The protocol used to record EIS data is detailed in supplementary materials.

In all the experiments, a 12 cm² (200 mm-long by 6 mm-wide) single cell was used to validate the model. It comprises two parallel channels of 200 mm-long by 1.5 mm-deep. At the cathode side, the flow field was machined directly in the copper current collector to enable an optical access inside the channels via a transparent plexiglass plate inserted on the top of the channels (see Fig. 2(b)). The current collector was gold plated to ensure minimal ohmic resistance (and large W_a). Between the current collectors, a membrane electrode assembly (MEA) was inserted; it is made of a 15 μm -thick Gore PEM with 0.5 mg/cm² platinum loading in both anode and cathode CL. The very thin membrane and high platinum loading were specially chosen to ensure low membrane resistance and efficient electrochemical reaction which match our model assumptions (negligible ohmic losses in the membrane and no overpotential gradients in the CL). The MEA was sandwiched between two 10BC GDLs from SGL® compressed at 250 μm using two rigid spacers.

Table 1
Geometrical characteristics of the segmented current collector.

Segment #	1	2	3	4	5	6	7	8	9	10	11
Length (mm)	19	18	18	18	18	18	18	18	18	18	19
Area (cm ²)	1.14	1.08	1.08	1.08	1.08	1.08	1.08	1.08	1.08	1.08	1.14
Dimensionless position	0.95	0.86	0.77	0.68	0.59	0.50	0.41	0.32	0.23	0.14	0.05

Finally, two aluminum end-plates were used to assemble all the fuel cell components. A water cooling circuit connected to a temperature control system was drilled inside the end plates to keep the fuel cell temperature constant at 70 °C.

Hydrogen flow rate was kept constant throughout all the measurements at 300 ml/min, 70 °C and 30% relative humidity to ensure enough membrane hydration and negligible overpotential losses in the anode. The air flow rate was modulated based on the desired stoichiometry, but for all the experiments air enters fully dry at a fixed temperature of 70 °C at the cell inlet.

The oxygen stoichiometry and oxygen residence time are computed based on the experimental conditions. The mean air density in the cathode channel is estimated as follows:

$$\rho_{air} = \frac{P_{tot}}{RT} (x_{H_2O} M_{H_2O} + x_{O_2} M_{O_2} + x_{N_2} M_{N_2}), \quad (17)$$

with $x_{O_2} = 0.21$, $x_{N_2} = 0.79 - 0.21 x_{N_2}$ and $x_{N_2} + x_{O_2} + x_{H_2O} = 1$. Although the cell is fed using dry air, the water produced by the electrochemical reaction makes the air relative humidity close to 100%. Therefore, it is assumed that $x_{H_2O} = P_{sat}(T)/P_{tot}$. The relationship (15) is then used to compute the air flow rate at the cell temperature and pressure, i.e.: $\dot{Q}(T, p) = \dot{Q}_{SCPT} \cdot \rho_{SCPT} / \rho_{air}$ where \dot{Q}_{SCPT} and ρ_{SCPT} are the flow rate and the density of air in standard condition of pressure and temperature. Then, the oxygen stoichiometry is obtained as

$$\lambda = \frac{\dot{Q}(T, p) c^{ref}}{I_{cell} / (4F)}, \quad (18)$$

where $\dot{Q}(T, p)$ is the volume flow rate given for the cell operating pressure and temperature, I_{cell} is the cell operating current, and c^{ref} is the oxygen concentration at the channel inlet given by the ideal gas law as:

$$c^{ref} = x_{O_2}^{inlet} \frac{P_{tot}}{RT}, \quad (19)$$

where $x_{O_2}^{inlet}$ is the inlet oxygen mole fraction taken to be 0.21 as dry air is used, and p_{tot} is the total air pressure in the fuel cell.

The model derived in section 2.1 is based on a two-dimensional (2D) geometry which does not take into account the effect of the ribs. Therefore, the velocity defined in Equation (1) is a 2D velocity that would flow without any rib. Experimentally the 2D velocity is given by

$$u_c^{2D} = \frac{\dot{Q}(T, p)}{l_c h_c}, \quad (20)$$

where l_c is the cell width, e.g. 6 mm. Finally, the oxygen residence time is based on the u_c^{2D} as

$$\tau_c = \frac{L_c}{u_c^{2D}}. \quad (21)$$

In our flow field geometry, the ratio of the cell active surface to the channel surface is 0.5, thus u_c^{2D} is equal to the half the 3D velocity that flows inside the fuel cell channels.

3. Results & discussion

3.1. Multiscale evidence of the stoichiometric regime

Before to be able to use the stoichiometric model to characterize the

fuel cell electrochemical kinetics, evidences of the stoichiometric regimes have to be observed. This was done at the previously mentioned scales: at the global scale where the EIS signatures at low frequency are measured and at the local scale based on the current density distribution measurements.

3.1.1. At the global scale using low frequency EIS measurements

Like in the authors' previous works [16], the low frequency EIS signature is used to evidence the stoichiometric regime. In the previous section, it was shown that the low frequency phase in the stoichiometric regime is a function of τ_c and λ (see Equation (15)), so it can be predicted easily knowing the fuel cell operating conditions. The low frequency fuel cell phase is measured from the fuel cell impedance as follows:

$$\tan\phi_{exp} = \frac{\text{Im}(Z_{exp})}{\text{Re}(Z_{exp}) - r_{HF}} \quad (22)$$

where Z_{exp} is the measured fuel cell impedance, and r_{HF} is the high frequency resistance taken as the average of the real part of the fuel cell impedance between 10 Hz and 5 kHz. r_{HF} is subtracted from the fuel cell impedance to match the assumption of negligible charge transport in the model. The fuel cell phase is measured for a range of oxygen stoichiometries and fuel cell currents. Details about the operating conditions used can be found in Table (2).

The comparison between Equation (15) and the low frequency phase measurements (Equation (22)) for a range of oxygen stoichiometries and a range of currents is presented in Fig. 3. The model is computed for the stoichiometry at which the cell is operating (see Equation (18)) and an interval at $\pm 10\%$ of this oxygen stoichiometry is depicted in dash line. To validate that the cell is operating in stoichiometric regime one can

expect that the measured fuel cell phases fall within this interval. As it can be observed in Fig. 3, this is particularly true at $\lambda = 1.30$ and 1.60 for all the currents (0.25, 0.375 and 0.5 A/cm²). However, more deviation is noticed at $\lambda = 2.15$, and the measured phase is out of the interval at $\lambda = 3.15$. Therefore, it can be concluded that the cell is operating in stoichiometric regime for a range of stoichiometric from 1.30 to 2.15 for all the currents tested. This result is in line with the work reported in Ref. [16], and confirms that the assumption made concerning negligible ohmic losses in the membrane and the absence of overpotential gradient in the CL are valid.

Another interesting result concerns the scaling of all the measurements regardless the operating current used. This confirms that the low frequency phase depends only on the oxygen stoichiometry when plotted as a function of $\tilde{\omega}$. If the same data were plotted versus the angular frequency, the effect of the operating current would have been shown through a shift of the maximum of the fuel cell phase (see Ref. [16]).

3.1.2. At the local scale using current density distribution measurements

The same kind of evidence of the stoichiometric regime is now sought at the local scale. In the stoichiometric regime the current distribution is given by equation (9). If the measurements of the current in each segment follow the same distribution, then one can conclude that the fuel cell is operating in the stoichiometric regime.

The same operating conditions previously mentioned in Table 2 are used, and the results are presented in Fig. 4. The methodology to compute the error bars on the dimensionless currents is detailed in appendix. Globally, it can be noticed that the measurements agree well with the model regardless the operating currents used and the oxygen stoichiometries. For each stoichiometry, all the data points scale with the model with a very small dispersion with respect to the current level, concluding – once again – that only the stoichiometry governed the current distribution not the value of the current itself justifying the name of stoichiometric regime. Therefore, from the results presented in Fig. 4 and associated to those in Fig. 3, it is concluded that the fuel cell operates in stoichiometric regime for all the operating conditions given in Table 2.

As noticed in Fig. 4(d), surprisingly, the stoichiometric regime may still occur at $\lambda = 3.15$ also whereas it was not identified on the low frequency phase (see Fig. 3). This result may be due to some transients' phenomena which hinder the frequential signature such as oxygen transport delay in the GDL. When λ increases, τ_c also increases to the same order of magnitude than the characteristic time of the GDL oxygen transport (see Ref. [16]). Thus, it may be concluded that the measurements of the current density distribution would be a more reliable technique to evidence the stoichiometric regime since they are not perturbed by GDL transient phenomena.

The model and the measurements are observed to deviate the most at the cell extremities, i.e. at $\tilde{y} \approx 0.05$ and 0.95. At the channel inlet, air enters dry and become humidified after few millimetres. The membrane humidity could therefore be lower at the first segment leading to a lower

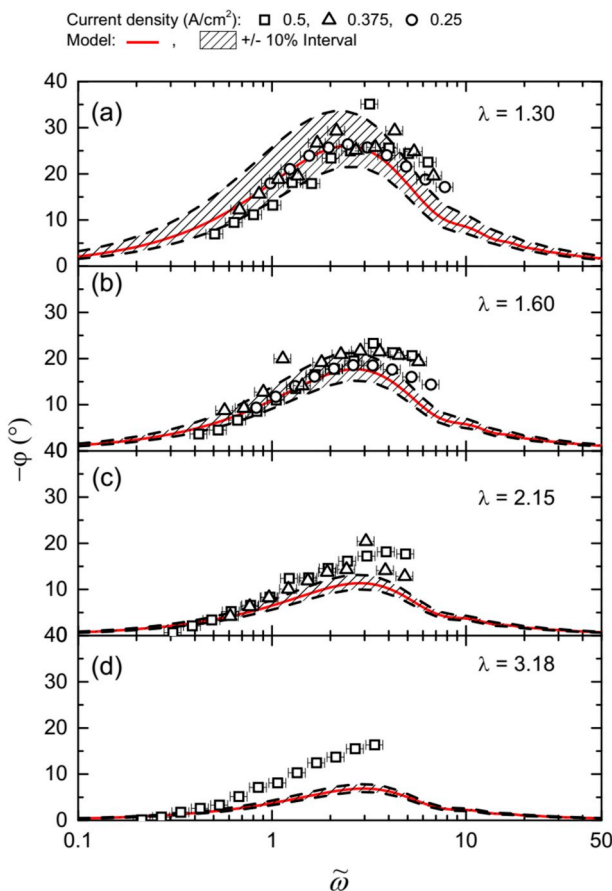


Fig. 3. Fuel cell low frequency phase measured by EIS for a range of current and oxygen stoichiometry.

Table 2
Summary of the operating conditions used in the stoichiometric regime.

Current density (A/cm ²)	Air flow rate (ml/min)	Pressure (bar)	ρ_{air} (kg/m ³)	u_c (m/s)	λ	τ_c
0.5	123	1.9	2.82	0.31	1.29	0.64
0.25	63	1.87	2.79	0.16	1.32	1.24
0.375	94	1.98	2.904	0.24	1.313	0.86
0.5	153	2.00	2.93	0.39	1.6	0.53
0.25	78	2.02	2.92	0.20	1.63	1.05
0.375	113	1.97	2.894	0.29	1.578	0.72
0.5	204	1.94	2.85	0.52	2.14	0.39
0.25	103	1.90	2.16	0.26	2.16	0.77
0.5	304	2.013	2.93	0.78	3.18	0.27

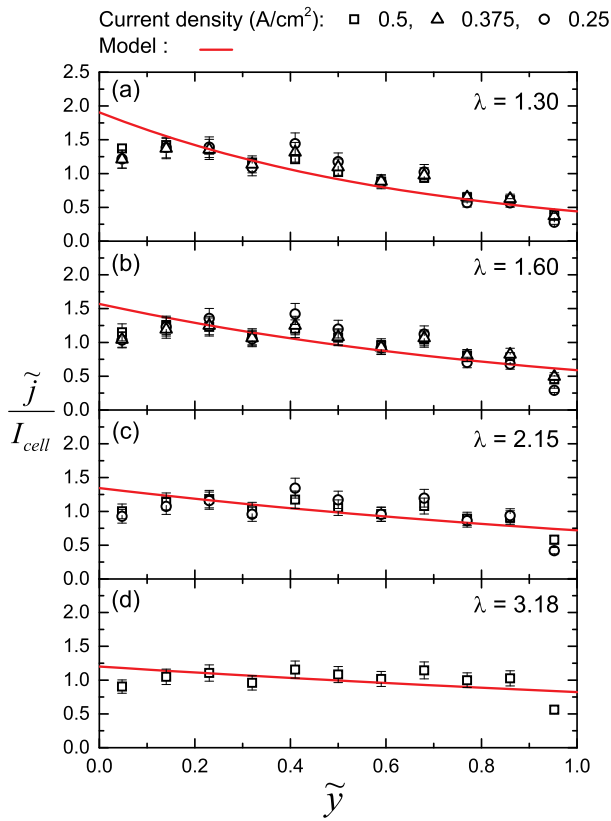


Fig. 4. Non-dimensional local current density distributions for a range of current and oxygen stoichiometry.

current production. This effect was observed in the literature on a larger scale [40,45], but here due to the very thin membrane used (15 μm), this non-uniform membrane humidity is only located at the first segment. A second source of uncertainty in the local current density measurement can stem from the uncertainty of the area of the MEA in the segments located at the extremities. During the fuel cell assembly with the segmented current collector, the MEA may have moved a bit toward one of the cell extremities (few millimetres) changing the surface area in contact with the segments at the extremities. This effect was pointed out by Kulkarni et al. [46] using X-rays radiography.

3.2. Characterisation of kinetic parameters in stoichiometric regime

3.2.1. Parameters identification

In the previous section, it was shown that the fuel cell is operating in the stoichiometric regime, validating the use of equations (1) and (2) to model the fuel cell behavior. Using these equations, one can show that $c_c^0(y)/c^{ref} = e^{-\lambda \tilde{y}}$, and $j_0 = i_c e^{\eta/b}$. Thus, by integrating equation (1) it leads to:

$$I_{cell} = \int_0^1 j(\tilde{y}) d\tilde{y} = i_c e^{\eta/b} \int_0^1 e^{-\lambda \tilde{y}} d\tilde{y} = \frac{i_c e^{\eta/b}}{\lambda \lambda^*}. \quad (23)$$

Equation (23), is then rewritten in linear form using the decimal logarithm to obtain:

$$\eta = 2.3b \times \log(I_{cell} \lambda \lambda^*) - 2.3b \times \log(i_c). \quad (24)$$

Equation (24) can be viewed as the Tafel equation but for a 2D cell where the current density I_{cell} is corrected by the effect of the stoichiometry in the channel, i.e. $\lambda \lambda^*$. Thus, by measuring the cell overpotential and current density, it is possible to accurately fit the Tafel slope and the exchange current density to characterize the cell electrochemical kinetics.

In Fig. 5, the overpotential measurement versus the corrected current density is shown for all the measurements summarised in Table 2. The methodology to compute the uncertainty of the current density is explained in appendix. The overpotential is computed as

$$\eta = 1.23 - E_{cell} - r_{HF} \times I_{cell}, \quad (25)$$

where E_{cell} , r_{HF} and I_{cell} are the cell voltage, ohmic resistance and current density measured. These values are summarised in Table 3. Using equation (24) and a linear regression, the Tafel slope and the exchange current are obtained (see Table 3 for the values).

In their review, Eslamibidgoli et al. [3] recalled that three regimes of electrochemical kinetics are theoretically expected. From medium to high overpotentials, these regimes are characterised by a value of Tafel slope that varies from 80 mV to 120 mV [3]. Our results presented in Fig. 5 show a similar trend where the slope varies between the data points measured at medium and high overpotential with a Tafel slope equal to 143 ± 21 mV and 229 ± 52 mV, respectively. We found that the value of the Tafel slope is larger than what is theoretically predicted, but the ratio between them is correct (2/3). The larger than expected Tafel slopes measured in his study are in-situ values in sense that some other physical phenomena may have impacted it: heterogeneities in the fuel cell assembly, effect of the channel/rib, catalyst degradations/aging. However, this Tafel slope can be considered as the correct values in the framework of the stoichiometric regime and become an accurate criterion to assess the kinetic performances of different fuel cell assemblies for example.

A similar conclusion can be drawn concerning the values of the exchange currents. We found two regimes at medium and high overpotential where the values of i_c vary significantly. Although it is difficult to link these in situ values to fuel cell characteristics (platinum loading, ECSA, catalyst layer composition ...), they can be used in the similar way as the Tafel slope: using i_c to characterize the fuel cell kinetics in the framework of the stoichiometric regime and compare them to study different catalyst layer or aging impact for example.

3.2.2. Model validation

Going further to validate the consistency of the measured value of b and i_c with the stoichiometric regime, we check the assumption made in section 2 where $\alpha_c = i_c/j_0 e^{\eta(t)/b} \approx 1$. In the stoichiometric regime, we can write that $\alpha_c = i_c e^{\eta/b} / (I_{cell} \lambda \lambda^*)$. These values are computed in Table 3. As it can be observed, α_c is found to be very close to 1 validating the assumption made earlier and meaning that the value b and i_c are

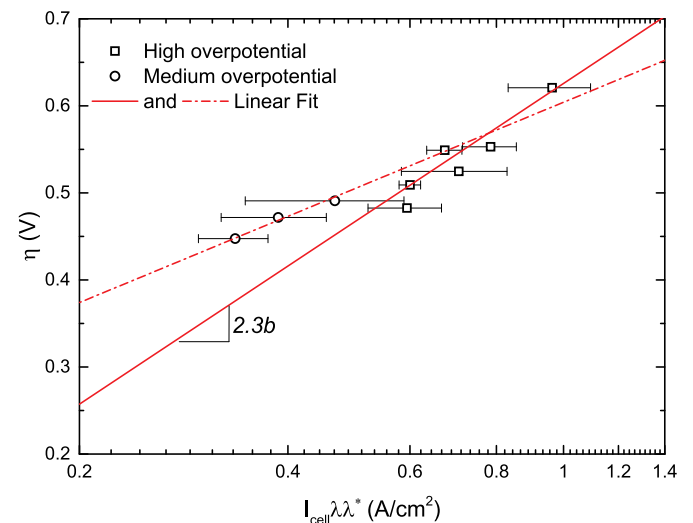


Fig. 5. Linear fit of the Tafel slope and exchange current density in the stoichiometric regime.

Table 3

Summary of the fuel cell characterisation in stoichiometric regime for a range of current and oxygen stoichiometry.

Current (A)	I_{cell} (A/cm ²)	λ	r_{HF} (m Ω)	E (V)	η (V)	b (mV)	s(mA/cm ²)	α_c
6	0.500	1.29	13	0.53	0.62	229 ± 52	65 ± 18	1,01
3	0.250	1.32	16	0.69	0.49	143 ± 21	21 ± 4	0,96
4.5	0.375	1.31	15	0.64	0.52	229 ± 52	65 ± 18	0,89
6	0.500	1.60	13	0.60	0.55	229 ± 52	65 ± 18	0,91
3	0.250	1.63	16	0.71	0.47	143 ± 21	21 ± 4	1,01
4.5	0.375	1.58	15	0.68	0.48	229 ± 52	65 ± 18	0,89
6	0.500	2.14	13	0.60	0.55	229 ± 52	65 ± 18	1,06
3	0.250	2.16	14	0.74	0.45	143 ± 21	21 ± 4	1,01
6	0.500	3.18	13	0.65	0.51	229 ± 52	65 ± 18	1,00

consistent with the assumptions made to derive the stoichiometric model.

The second validation is based on the fuel cell impedance modulus. Only the phase was used previously to verify that the fuel cell is operating in stoichiometric regime. To compute the dimensionless fuel cell impedance, $|Z_{exp}|$, the charge transfer resistance is needed as it is shown in Equation (16). The charge transfer resistance is given by $R_{ct} = b/(j_0)$ with $j_0 = I_{cell}\lambda\lambda^*$ according to Equation (23). The uncertainty associated to the dimensionless modulus is given in appendix. These data are presented in Fig. 6 and compared to the modulus of the impedance in stoichiometric regime given by Equation (14) as $|\tilde{Z}| = |1/\tilde{Z}|^{-1}$.

The experimental modulus measured in stoichiometric regime scales quite well with the model (red lines in Fig. 6) for all the oxygen stoichiometries. Although some deviations can be observed (at $\lambda = 2.15$ and 3 A for example), the general trend is well reproduced. This result shows that the fuel cell can be fully characterized where all the parameters of the stoichiometric regime can be measured (membrane resistance, electrochemical kinetics, oxygen transport in the channel) and used to predict both the steady state of the cell (current and current density) and periodic state (fuel cell impedance).

4. Conclusions

The aim of this paper was to evidence the stoichiometric regime in an operating fuel cell both at the global and local scale using EIS measurements and current density distribution measurements with a segmented flow field. This was successfully done for a range of stoichiometry from 1.30 to 3.18 and a range of current from 3 A to 6 A (0.25–0.5 A/cm²). At the local scale it may have been easier to evidence the stoichiometric regime, particularly at $\lambda = 3.18$ where the low frequency phase can be altered by the oxygen transport in the GDL (see Ref. [16]). However, the use of segmented cell is not mandatory to obtain a signature of the stoichiometric regime since it is well observed through the low frequency phase for most of the measurements presented in this paper.

Operating a fuel cell in this particular regime is a great advantage from the modelling point of view as only two equations govern the main physical mechanisms. Therefore, few parameters are needed to predict the fuel cell behavior. Moreover, in the case they are not known, such as the kinetics parameters (Tafel slope and exchange current), a methodology is presented to measure them accurately. Thus, within the framework of this stoichiometric regime, PEM fuel cells can be better controlled, their performances better predicted, and their physical properties better characterized.

Another application of these works concerns the hydrogen/oxygen fuel cells where mass transport in the GDL are not limiting. Thus, these fuel cells operating conditions fall within the assumption needed to derive the stoichiometric regime, and our work can be transposed to this

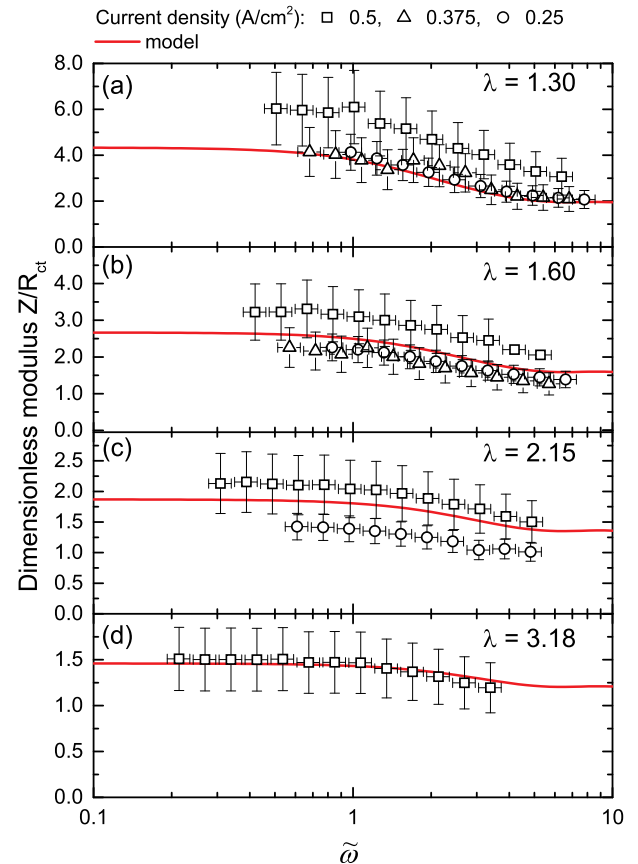


Fig. 6. Impedance modulus versus dimensionless frequency for a range of air stoichiometry and cell current.

technology to characterize the kinetic parameters or to control hydrogen/oxygen fuel cell performances.

Acknowledgements

The research leading to these results received funding from the People Programme (Marie Curie Actions) of the European Union's Seventh Framework Programme (FP7/2007–2013) under REA grant agreement n° PCOFUND-GA-2013-609102, through the PRESTIGE programme coordinated by Campus France. The authors would like to gratefully acknowledge Mr Christophe Le Bozec for his help in designing and building the experimental setup.

Appendix. Uncertainty calculations

Dimensionless current

We consider that the N current densities measured by the segmented current collector are known within $\pm 10\%$ of the measured value. So, the uncertainty on the mean value is:

$$u_{mean} = \frac{0.1}{N} \sqrt{\sum_{n=1}^N j_n^2}, \quad (\text{A.1})$$

This is the root sum of squares of the measured current density.

Thus, one can deduce that the uncertainty of the dimensionless current is:

$$u_{I_{adim}} = 0.1 I_{adim} \sqrt{1 + \frac{\sum_{n=1}^N j_n^2}{N^2 I_{mean}^2}}, \quad (\text{A.2})$$

Flow rate, velocity and stoichiometry

In this study, the air flow rate, velocity and stoichiometry are considered to be known at $\pm 10\%$. This uncertainty stems from the mass flow controller, the cell temperature controller and the back pressure controller. For sake of simplicity, all these uncertainties are embedded in a single one where the velocity is assumed to be known at $\pm 10\%$ of u_c .

Tafel slope

Calculation of the uncertainty on the Tafel slope and the exchange current density obtained from the linear fit. For the Tafel slope, it is trivial: $u_b = u_{a_1}/2.3$ where u_{a_1} is the uncertainty computed by the linear fit including the weight of each data (error bar on x-axis). Concerning the exchange current, it is given by the following formula: $i_c = 10^{-a_2/a_1}$ where a_1 and a_2 are the slope and the intercept, respectively. Thus, the uncertainty on i_c is given by:

$$u_{i_c}^2 = \left(u_{a_1} \frac{\partial i_c}{\partial a_1}\right)^2 + \left(u_{a_2} \frac{\partial i_c}{\partial a_2}\right)^2, \quad (\text{A.3})$$

which lead to

$$u_{i_c} = i_c \sqrt{\frac{u_{a_2}^2}{a_2^2} + \frac{u_{a_1}^2}{a_1^2} \frac{a_2^2}{a_1^2}}. \quad (\text{A.4})$$

Modulus

The uncertainty of the modulus depends of the uncertainty of the charge transfer resistance computed as:

$$u_{R_{ct}}^2 = \left(\frac{u_b}{\lambda \lambda^* I_{cell}}\right)^2 + u_{I_{cell}}^2 \frac{b^2}{I_{cell}^2} \left(\frac{(1-\lambda)\lambda^* + 1}{(1-\lambda)\lambda^{*2}\lambda^2}\right)^2, \quad (\text{A.5})$$

which lead to

$$\frac{u_{R_{ct}}^2}{R_{ct}^2} = \left(\frac{u_b}{b}\right)^2 + \frac{u_{\lambda}^2}{\lambda^2} \left(\frac{(1-\lambda)\lambda^* + 1}{(1-\lambda)\lambda^*}\right)^2. \quad (\text{A.6})$$

where $u_{\lambda} = 0.1 \times \lambda$ and u_b is given in Table 3. Finally, one can obtain

$$u_{R_{ct}} = R_{ct} \sqrt{\left(\frac{u_b}{b}\right)^2 + 0.1^2 \left(\frac{(1-\lambda)\lambda^* + 1}{(1-\lambda)\lambda^*}\right)^2}, \quad (\text{A.7})$$

and, the uncertainty on the dimensionless modulus is given by

$$u_{|\tilde{Z}|} = |\tilde{Z}| \frac{u_{R_{ct}}}{R_{ct}}. \quad (\text{A.8})$$

Appendix A. Supplementary data

Supplementary data to this article can be found online at <https://doi.org/10.1016/j.jpowsour.2019.227100>.

References

- [1] N. Konno, S. Mizuno, H. Nakaji, Y. Ishikawa, Development of compact and high-performance fuel cell stack, *SAE Int. J. Altern. Powertrains*. 4 (1) (2015) 123–129, <https://doi.org/10.4271/2015-01-1175>, 01–1175.
- [2] T. Yoshida, K. Kojima, Toyota MIRAI fuel cell vehicle and progress toward a future hydrogen society, *Interface Mag* 24 (2015) 45–49.
- [3] M.J. Eslamibidgoli, J. Huang, T. Kadyk, A. Malek, M. Eikerling, How theory and simulation can drive fuel cell electrocatalysis, *Nano Energy* 29 (2016) 334–361.
- [4] A.Z. Weber, R.L. Borup, R.M. Darling, P.K. Das, T.J. Dursch, W. Gu, et al., A critical review of modeling transport phenomena in polymer-electrolyte fuel cells, *J. Electrochem. Soc.* 161 (2014) F1254–F1299.
- [5] A.Z. Weber, J. Newman, Modeling transport in polymer-electrolyte fuel cells, *Chem. Rev.* 104 (2004) 4679–4726.
- [6] A.A. Kulikovskiy, The effect of stoichiometric ratio λ on the performance of a polymer electrolyte fuel cell, *Electrochim. Acta* 49 (2004) 617–625.
- [7] J.T. Gostick, Versatile and efficient pore network extraction method using marker-based watershed segmentation, *Phys. Rev. E*. 96 (2017), 023307.
- [8] L. Cindrella, A.M. Kannan, J.F. Lin, K. Saminathan, Y. Ho, C.W. Lin, J. Wertz, Gas diffusion layer for proton exchange membrane fuel cells—a review, *J. Power Sources* 194 (2009) 146–160.
- [9] G. Zhang, K. Jiao, Multi-phase models for water and thermal management of proton exchange membrane fuel cells: a review, *J. Power Sources* 391 (2018) 120–133.
- [10] B.P. Setzler, T.F. Fuller, A physics-based impedance model of proton exchange membrane fuel cells exhibiting low-frequency inductive loops, *J. Electrochem. Soc.* 162 (2015) F519–F530.
- [11] Y. Wang, S. Basu, C.-Y. Wang, Modeling two-phase flow in PEM fuel cell channels, *J. Power Sources* 179 (2008) 603–617.
- [12] T.E. Springer, T.A. Zawodzinski, S. Gottesfeld, Polymer electrolyte fuel cell model, *J. Electrochem. Soc.* 138 (1991) 2334.
- [13] A.A. Kulikovskiy, A simple equation for in situ measurement of the catalyst layer oxygen diffusivity in PEM fuel cell, *J. Electroanal. Chem.* 720–721 (2014) 47–51.
- [14] A.A. Kulikovskiy, The regimes of catalyst layer operation in a fuel cell, *Electrochim. Acta* 55 (2010) 6391–6401.
- [15] S. Chevalier, C. Josset, B. Auvity, Analytical solutions and dimensional analysis of pseudo 2D current density distribution model in PEM fuel cells, *Renew. Energy* 125 (2018) 738–746.
- [16] S. Chevalier, C. Josset, B. Auvity, Analytical solution for the low frequency polymer electrolyte membrane fuel cell impedance, *J. Power Sources* 407 (2018) 123–131.
- [17] J. Xuan, H. Wang, D.Y.C. Leung, M.K.H. Leung, H. Xu, L. Zhang, Y. Shen, Theoretical Graetz–Damköhler modeling of an air-breathing microfluidic fuel cell, *J. Power Sources* 231 (2013) 1–5.
- [18] G. Maranzana, J. Mainka, O. Lottin, J. Dillet, A. Lamibrac, A. Thomas, S. Didierjean, A proton exchange membrane fuel cell impedance model taking into account convection along the air channel: on the bias between the low frequency limit of the impedance and the slope of the polarization curve, *Electrochim. Acta* 83 (2012) 13–27.
- [19] K.T. Jeng, C.P. Kuo, S.F. Lee, Modeling the catalyst layer of a PEM fuel cell cathode using a dimensionless approach, *J. Power Sources* 128 (2004) 145–151.
- [20] O. Shamardina, M.S. Kondratenko, A.V. Chertovich, A. Kulikovskiy, A simple transient model for a high temperature PEM fuel cell impedance, *Int. J. Hydrogen Energy* 39 (2014) 2224–2235.
- [21] J.-C. Olivier, G. Wasselynck, S. Chevalier, B. Auvity, C. Josset, D. Trichet, G. Squadrito, N. Bernard, Multiphysics modeling and optimization of the driving strategy of a light duty fuel cell vehicle, *Int. J. Hydrogen Energy* 42 (2017) 26943–26955.
- [22] N. Fouquet, C. Doulet, C. Nouillant, G. Dauphin-Tanguy, B. Ould-Bouamama, Model based PEM fuel cell state-of-health monitoring via ac impedance measurements, *J. Power Sources* 159 (2006) 905–913.
- [23] I. Manke, C. Hartnig, M. Grünerbel, W. Lehnert, N. Kardjilov, A. Haibel, A. Hilger, J. Banhart, H. Riesemeier, Investigation of water evolution and transport in fuel cells with high resolution synchrotron x-ray radiography, *Appl. Phys. Lett.* 90 (2007) 174105.
- [24] J. Lee, S. Chevalier, R. Banerjee, P. Antonacci, N. Ge, R. Yip, T. Kotaka, Y. Tabuchi, A. Bazylak, Investigating the effects of gas diffusion layer substrate thickness on polymer electrolyte membrane fuel cell performance via synchrotron X-ray radiography, *Electrochim. Acta* 236 (2017) 161–170.
- [25] D. Hayashi, A. Ida, S. Magome, T. Suzuki, S. Yamaguchi, R. Hori, Synchrotron X-Ray Visualization and Simulation for Operating Fuel Cell Diffusion Layers, 2017.
- [26] Q. Meyer, Y. Zeng, C. Zhao, In situ and operando characterization of proton exchange membrane fuel cells, *Adv. Mater.* (2019) 1901900.
- [27] G. Hinds, In situ diagnostics for polymer electrolyte membrane fuel cells, *Curr. Opin. Electrochem.* 5 (2017) 11–19.
- [28] J.E.B. Randles, Kinetics of rapid electrode reactions, *Discuss. Faraday Soc.* 1 (1947) 11–19.
- [29] P. Antonacci, S. Chevalier, J. Lee, N. Ge, J. Hinebaugh, R. Yip, Y. Tabuchi, T. Kotaka, A. Bazylak, Balancing mass transport resistance and membrane resistance when tailoring MPL thickness for PEM fuel cells, *Electrochim. Acta* 188 (2016) 888–897.
- [30] T.E. Springer, T.A. Zawodzinski, M.S. Wilson, S. Gottesfeld, Characterization of polymer electrolyte fuel cells using AC impedance spectroscopy, *J. Electrochem. Soc.* 143 (1996) 587–599.
- [31] D. Kramer, I.A. Schneider, A. Wokaun, G.G. Scherer, Oscillations in the gas channels - the forgotten player in impedance spectroscopy in polymer electrolyte fuel cells B. Modeling the wave, in: E.C.S. Trans. (Ed.), ECS, 2006, pp. 1249–1258.
- [32] S.M. Rezaei Niya, M. Hoorfar, Study of proton exchange membrane fuel cells using electrochemical impedance spectroscopy technique – a review, *J. Power Sources* 240 (2013) 281–293.
- [33] L.C. Pérez, L. Brandão, J.M. Sousa, A. Mendes, Segmented polymer electrolyte membrane fuel cells—a review, *Renew. Sustain. Energy Rev.* 15 (2011) 169–185.
- [34] I.A. Schneider, D. Kramer, A. Wokaun, G.G. Scherer, Oscillations in gas channels: II. Unraveling the characteristics of the low frequency loop in air-fed PEFC impedance spectra, *J. Electrochem. Soc.* 154 (2007) B770–B782.
- [35] Q. Meyer, K. Ronaszegi, J.B. Robinson, M. Noorkami, O. Curnick, S. Ashton, A. Danelyan, T. Reisch, P. Adcock, R. Kraume, P.R. Shearing, D.J.L. Brett, Combined current and temperature mapping in an air-cooled, open-cathode polymer electrolyte fuel cell under steady-state and dynamic conditions, *J. Power Sources* 297 (2015) 315–322.
- [36] T. Reshetenko, A. Kulikovskiy, Comparison of two physical models for fitting PEM fuel cell impedance spectra measured at a low air flow stoichiometry, *J. Electrochem. Soc.* 163 (2016) F238–F246.
- [37] N. Zamel, A. Bhattacharai, D. Gerteisen, Measurement of spatially resolved impedance spectroscopy with local perturbation, *Fuel Cells* 13 (2013) 910–916.
- [38] G. Maranzana, O. Lottin, T. Colinar, S. Chupin, S. Didierjean, A multi-instrumented polymer exchange membrane fuel cell: observation of the in-plane non-homogeneities, *J. Power Sources* 180 (2008) 748–754.
- [39] A. Kulikovskiy, Analytical impedance of oxygen transport in a PEM fuel cell channel, *J. Electrochem. Soc.* 166 (2019) F306–F311.
- [40] I.A. Schneider, S.A. Freunberger, D. Kramer, A. Wokaun, G.G. Scherer, Oscillations in gas channels. Part I. The forgotten player in impedance spectroscopy in PEFCs, *J. Electrochem. Soc.* 154 (2007) B383–B388.
- [41] I. Pivac, F. Barbir, Inductive phenomena at low frequencies in impedance spectra of proton exchange membrane fuel cells – a review, *J. Power Sources* 326 (2016) 112–119.
- [42] I.J. Halvorsen, I. Pivac, D. Bezmalinović, F. Barbir, F. Zenith, Electrochemical low-frequency impedance spectroscopy algorithm for diagnostics of PEM fuel cell degradation, *Int. J. Hydrogen Energy* (2019).
- [43] S. Chevalier, N. Ge, J. Lee, M.G. George, H. Liu, P. Shrestha, D. Muirhead, N. Lavielle, B.D. Hatton, A. Bazylak, Novel electrospun gas diffusion layers for polymer electrolyte membrane fuel cells: Part II. In operando synchrotron imaging for microscale liquid water transport characterization, *J. Power Sources* 352 (2017) 281–290.
- [44] T. Reshetenko, A. Kulikovskiy, On the distribution of local current density along a PEM fuel cell cathode channel, *Electrochem. Commun.* 101 (2019) 35–38.
- [45] A.A. Kulikovskiy, Semi-analytical 1D+1D model of a polymer electrolyte fuel cell, *Electrochem. Commun.* 6 (2004) 969–977.
- [46] N. Kulkarni, Q. Meyer, J. Hack, R. Jervis, F. Iacoviello, K. Ronaszegi, P. Adcock, P. R. Shearing, D.J.L. Brett, Examining the effect of the secondary flow-field on polymer electrolyte fuel cells using X-ray computed radiography and computational modelling, *Int. J. Hydrogen Energy* 44 (2019) 1139–1150.